Effects of Ni and Cr on Cryogenic Impact Toughness of Bainite/Martensite Multiphase Steels

Zishan Yao[1] · Guang Xu[1] · Zhengyi Jiang[2] · Junyu Tian[1] · Qing Yuan[1] · Hongwei Ma[1]

Abstract

In the present research, the effects of Nickel (Ni) and Chromium (Cr) on cryogenic impact toughness (CIT) of low-carbon bainite/martensite multiphase steels [processed by two different cooling processes: isothermal transformation process (ITP) and continuous cooling process (CCP)] were investigated. It was found that due to the formation of carbides during isothermal treatment, the addition of Ni and Cr yielded no significant improvements in CIT. However, during CCP treatment, the addition of Ni manifested a considerable enhancement in CIT, whereas the addition of both Ni and Cr caused a decrease in CIT. Further, after ITP treatment, the microstructure of all steels consisted of bainite and martensite, while Ni + Cr steel contained the largest amount of bainite. The microstructures of the CCP-treated steels mainly also consisted of bainite and martensite, but no retained austenite and carbides were observed, thus resulting in a superior CIT.

Keywords Cryogenic impact toughness · Bainite/martensite multiphase steels · Nickel · Chromium · Microstructure

Abbreviations

CIT	Cryogenic impact toughness
ITP	Isothermal transformation process
CCP	Continuous cooling process
Ni	Nickel
Cr	Chromium
Bs	Starting temperature of bainitic transformation
Ms	Starting temperature of martensitic transformation
SEM	Scanning electron microscope
TEM	Transmission electron microscope
XRD	X-ray diffraction
RA	Retained austenite
M	Martensite
BF	Bainitic ferrite
TM	Tempered martensite
TC	Tempered carbide
M/A	Martensite and austenite
GB	Granular bainite
LM	Lath martensite
AM	Prior martensite
FM	Fresh martensite
Mn	Manganese

✉ Guang Xu
xuguang@wust.edu.cn

1 The State Key Laboratory of Refractories and Metallurgy, Wuhan University of Science and Technology, Mail Box 131, 947 Heping Avenue, Qingshan District, Wuhan 430081, Hubei, China

2 School of Mechanical, Materials, Mechatronic and Biomedical Engineering, University of Wollongong, Wollongong, NSW 2522, Australia

1 Introduction

With the continuous progress of society and economic development, and the demands of environment protection and energy saving has put a more stringent requirement for high strength steels with improved mechanical properties and low cost. Traditional martensitic steels are widely used as wear-resistant steel, high-strength structural steel, and tool steel etc. [1–3]. Although martensitic steels possess high strength and hardness, their toughness and plasticity are relatively poor [4, 5]. In recent years, nanostructured bainitic steels have attracted considerable attention due to their extremely high strengths (~2.5 GPa) and much higher toughness as compared to martensitic steels [6–8].

It has already proved that both tempered martensite structure and isothermal bainite structure manifest excellent toughness [9–11]. Isothermal bainite/martensite multiphase structures generally possess significantly higher toughness than that of the single phase structure of tempered martensite or isothermal bainite [12–14]. However, due to long isothermal process

and high energy consumption, their practical applications in engineering industries are still limited. The continuous cooling technology can effectively shorten treatment time and save energy; therefore, it is worthwhile to investigate the effects of continuous cooling on microstructural and mechanical properties of bainite/martensite dual-phase steels.

It is well known that the addition of Nickel (Ni) in steels enlarges the austenite phase region, inhibits bainitic transformation, decreases the ductile–brittle transition temperature, and effectively improves cryogenic impact toughness (CIT) [15–17]. In contrast, Chromium (Cr) dissolves into Fe matrix, shrinks the austenite phase region, and promotes bainitic transformation [18]. Therefore, the addition of Cr in steels yields profound improvements in strength and hardness and at the same time, causes a significant increase in ductile-brittle transition temperature [19, 20]. Moreover, high Cr contents significantly decrease the impact toughness of steels due to the precipitation of δ-phase [21]. However, there are fewer investigations on the effects of addition of Ni and Cr on microstructure and toughness of bainite/martensite dual-phase steels, especially on the CIT at isothermal transformation process (ITP) and continuous cooling process (CCP).

In the present study, two different cooling processes, i.e. isothermal transformation process and continuous cooling process, were adopted to prepare low-carbon bainite/martensite multiphase steels of three different chemical composition (base steel (without Ni and Cr), Ni-steel, and Ni+Cr steel). Further, the effects of different cooling processes on microstructures, low-temperature impact energies, hardness, and CIT of the as-prepared bainite/martensite dual-phase steels were investigated in detail. The research results can provide theoretical reference for the production of bainite/martensite dual-phase steels.

2 Materials and Methods

The chemical compositions of all three experimental steels are presented in Table 1. The base steel without Ni and Cr was used to compare with other two steels. The theoretical starting temperature of bainitic transformation (Bs) and the starting temperature of martensitic transformation (Ms) of the steels were determined by MUCG 83 software developed by Bhadeshia at Cambridge University [22, 23].

The test steels were refined in a 50 kg vacuum furnace and then cast into ingots. The hot-rolled (thickness of 12 mm) plates were water-cooled to 500 °C and then air-cooled to room temperature. The thermal simulation specimens of

$11 \, mm \times 11 \, mm \times 85 \, mm$ size were cut from the plates along the rolling direction, and the top and the bottom surfaces of the specimens were conventionally polished. The thermal simulation experiments were implemented in a Gleeble-3800 thermal-mechanical simulator (Fig. 1). All specimens were first heated to 950 °C at 10 °C/s for 10 min for austenitization and then fast-cooled to 380°C at 20 °C/s. The cooling rate of 20 °C/s was high enough to avoid high-temperature transformations, such as ferrite and pearlite transformations. In order to compare the influences of different cooling processes on CIT of the specimens, two cooling processes (ITP and CCP) were carried out after 380 °C. During ITP, the specimens were held at 380 °C for 30 min and then cooled to room temperature at 5 °C/s, whereas the CCP specimens were directly cooled to room temperature from 380 °C at 5 °C/s. In all cases, the change in diameter of the specimens during cooling was recorded using a thermal dilatometer.

After the thermal simulation experiment, the specimens were machined into 55 mm × 10 mm × 10 mm size to perform the V-notch Charpy impact test (Impact machine model: JSCJ300–1) at −40 °C and fracture surfaces were analyzed by a Zeiss Sigma 300 scanning electron microscope (SEM). The hardness values of the specimens under 5 kg load were measured by an MHVS–50Z Vickers hardness tester equipped with a pyramid-shaped diamond indenter. In addition, metallographic samples were first cut from the soaking zone of each thermal simulation specimen, then mounted and grounded with abrasive papers of 400-grit, 800-grit, 1200-grit, 1500-grit, and 2000-grit, then polished with 1.5 μm diamond paste, and finally etched by
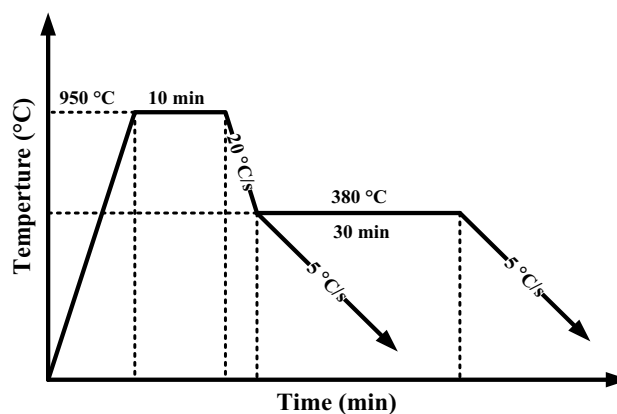

Fig. 1 The schematic illustration of experimental procedures

Table 1 Chemical composition (wt%) and Ms, Bs (°C) of three test steels

Steel	C	Si	Mn	Mo	Cr	Ni	P	S	Ms	**Bs**
Base	0.22	0.41	2.00	0.19	–	–	0.008	0.0029	376	517
Ni	0.24	0.42	2.08	0.20	–	1.50	0.005	0.0024	349	488
Ni+Cr	0.25	0.42	2.04	0.22	1.63	1.50	0.010	0.0030	308	439

4% nital, and the microstructures of the as-prepared samples were observed by a Nova 400 SEM. Moreover, the thin foils samples for transmission electron microscope (TEM) observations were prepared by a twin-jet polishing technique using an electrolyte containing perchloric aicd (6%) and ethanol (94%) and the microstructures were observed by a JEM-2100F TEM. The X-ray diffraction (XRD) analysis was performed to measure the volume fraction of retained austenite (RA) by an Empyrean diffractometer with Co-Kα radiation with current of 50 mA and acceleration voltage of 35 kV.

3 Results and Discussion

3.1 SEM Analysis

The microstructures of all steel specimens were analyzed by SEM (Fig. 2). It is noticeable that the microstructures of the samples mainly consisted of martensite (M) and bainitic ferrite (BF). After ITP treatment, tempered martensite (TM) and some lath-like BF were detected in the microstructure

of the base steel. Moreover, tempered carbide (TC) was found to be uniformly distributed on the martensite surface (Fig. 2a). It can be seen from Fig. 2b, as compared to the base steel, Ni-steel yielded a higher amount of lath-like bainite, which were distributed in parallel at different orientations in the grains. The original austenite grains were divided by BF plates. M and small amounts of martensite and austenite (M/A) islands were observed in Ni-steel. After isothermal treatment, austenite grains in Ni + Cr steel were remarkably refined; however, large-sized M and granular bainite (GB) were observed in its microstructure (Fig. 2c). In comparison to Ni-steel, Ni + Cr steel yielded a lower amount of lath-like BF. The volume fractions of BF in three steels during ITP treatment can be calculated using the software of Image-Pro Plus [24].The micrographs of the Ni + Cr steel were shown in Fig. 3 as an example to show how to calculate the volume fraction of BF. The darker areas consisted of BF, M and M/A (Fig. 3a). First, the darker areas were automatically colored red by the software of Image-Pro Plus as shown in Fig. 3b. The area percentage of the red areas (labeled as A_1) was calculated by the software. Second, the darker blocky areas were M or M/A which were included
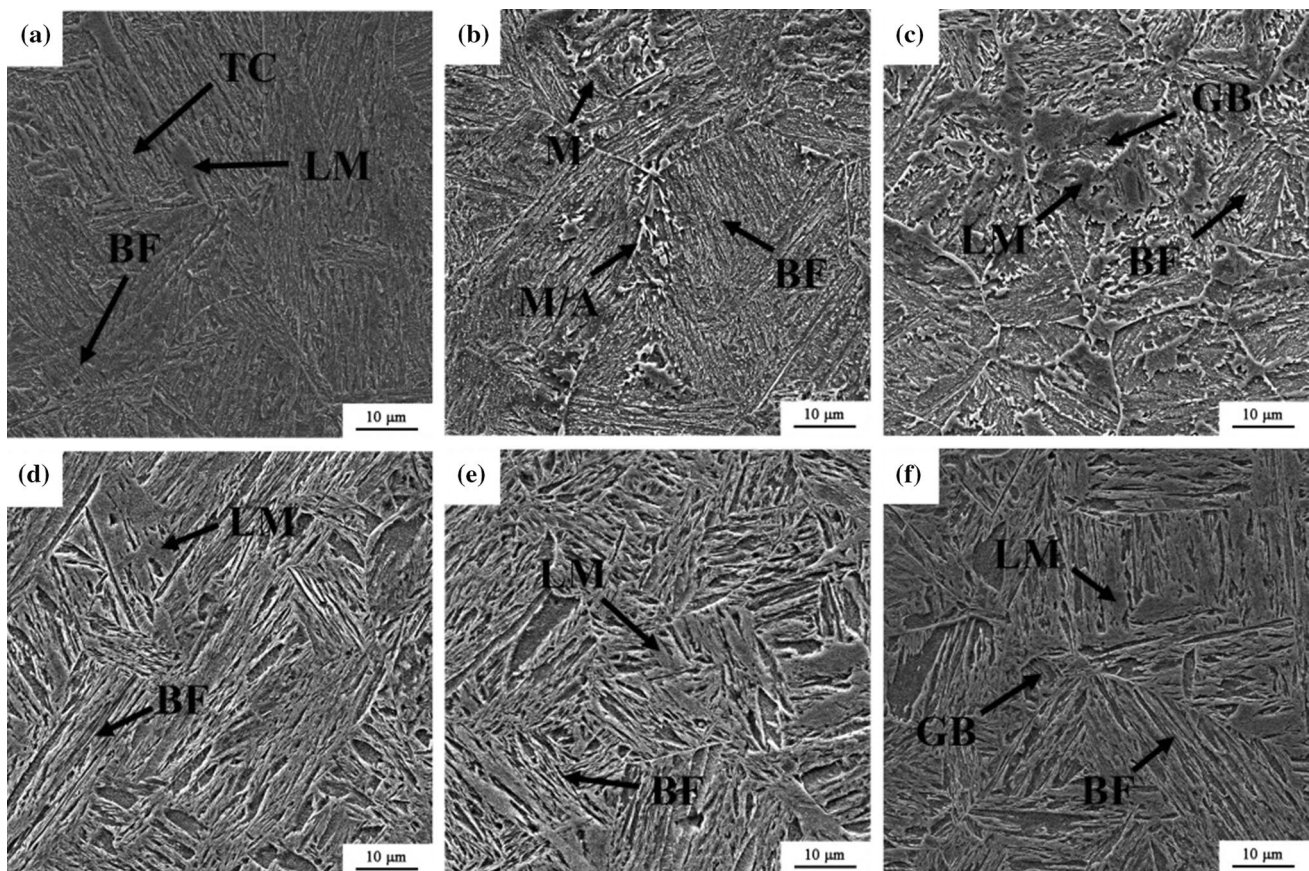

Fig. 2 SEM micrographs, for ITP treatment: **a** base steel; **b** Ni-steel; **c** Ni + Cr steel; and for CCP treatment: **d** base steel; **e** Ni-steel; **f** Ni + Cr steel

in A_1 and must be subtracted. The darker blocky areas were manually marked (Fig. 3c). The area percentage of these areas (labeled as A_2) was measured. Finally, the area percentage of bainite (labeled as A_3) was calculated by $A_3 = A_1 - A_2$. In this example, A1 was 71.44% and A2 was 23.78%, so that A3 was 47.66%. Therefore, the volume fraction of BF in Fig. 3 was 47.66%. In addition, the volume fractions of BF in base steel and Ni-steel during ITP treatment can be calculated by same method and the results were 7.72% and 44.25% respectively.

It is evident from Fig. 2d–f that all three steel samples manifested almost the same microstructure after CCP treatment. The microstructures of the CCP-treated samples mainly consisted of lath martensite (LM) and small amount of bainite, and no residual austenite and tempered carbides were observed. The amount of bainite in the CCP-treated samples was significantly lower than that of the ITP-treated samples. In comparison to the base steel, the lengths of LM and BF in Ni-steel were significantly reduced. In addition, it is obvious from Fig. 2e and f that the microstructures of Ni + Cr steel and Ni-steel were almost the same. Martensitic and bainite transformations mainly occurred in three steels during CCP treatment. According to authors' previous study [25], martensite consisted of prior martensite (PM) formed at the beginning stage of the whole cooling process and fresh martensite (FM) formed at later period of the whole cooling process. PM has the lower carbon content due to forming at higher temperature, resulting in better toughness. In addition, PM was easily etched and its microstructure morphology was concave (Fig. 4a). The micrograph of Ni-steel during CCP treatment was selected to calculate the volume fraction of PM. The darker concave areas were manually marked (Fig. 4b) and the area percentage of these areas was measured to be 23.66% by the software. Furthermore, the volume fractions of PM in base steel and Ni + Cr steel were

21.84% and 19.32% calculated by same method. The Ni + Cr steel had the smallest amount of PM, which was attributed to the lowest Ms temperature among three steels (Table 1).

3.2 XRD

The amounts of RA in the steel samples were measured by XRD (Table 2). No RA peaks were observed in the CCP-treated samples, thus indicating that all austenite completely transformed into M and BF. This result is consistent with SEM results (Fig. 2d–f). However, the ITP-treated Ni-steel and Ni + Cr steel contained very small amounts of RA (3% and 1%, respectively). Figure 5 presents the XRD test data of Ni-steel. In comparison to the base steel, Ni-steel contained more bainite. The bainitic transformation was accompanied by carbon partitioning into the surrounding untransformed austenite, thus resulting in an increase in chemical stability of untransformed austenite [26, 27].Therefore, the amount of RA in Ni-steel was found to be relatively higher than that of the base steel. In addition, Cr, as a strong carbide forming element, decreases the solubility of carbon atoms in austeniteand promotes carbide formation [28], thus resulting in a decrease in chemical stability of untransformed austenite in Ni + Cr steel. Therefore, the amount of RA in Ni + Cr steel was smaller than that in Ni-steel.

3.3 Thermal Dilatometry

The dilation amounts of the as-prepared steel samples were recorded by a Gleeble-3800 dilatometer. The beginning of isothermal holding at 380 °C during ITP and the beginning of air-cooling during CCP were selected as the zero point of the abscissa and the ordinate axes, respectively. The dilation curves were drawn in Origin 8.0 software (Fig. 6).
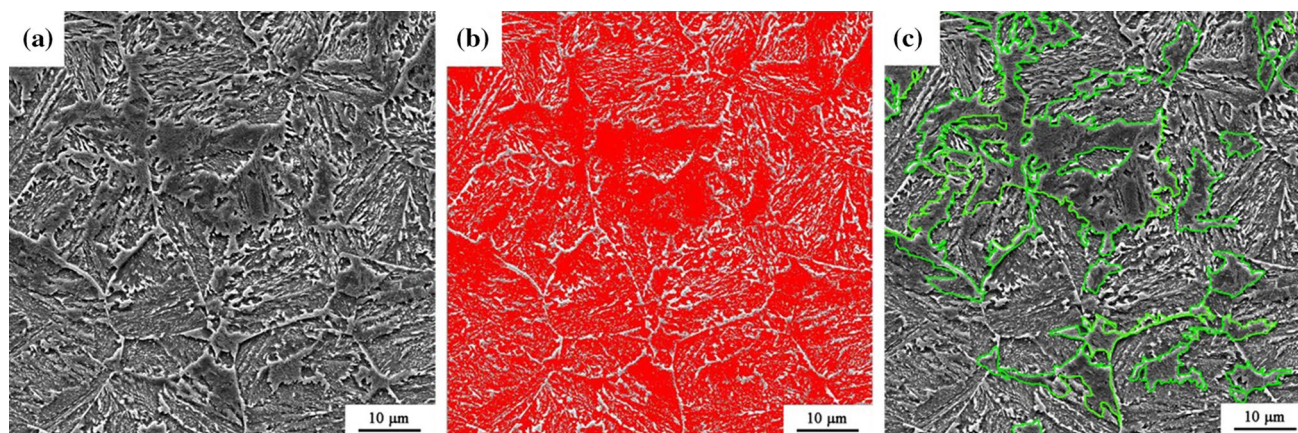

Fig. 3 The calculation of the volume fraction of BF in Ni + Cr steel during ITP treatment: **a** the original graph; **b** the darker areas are colored red; **c** the darker blocky areas are marked

Fig. 4 The calculation of the volume fraction of AM in Ni-steel during CCP treatment: **a** the original graph; **b** the darker concave areas are marked
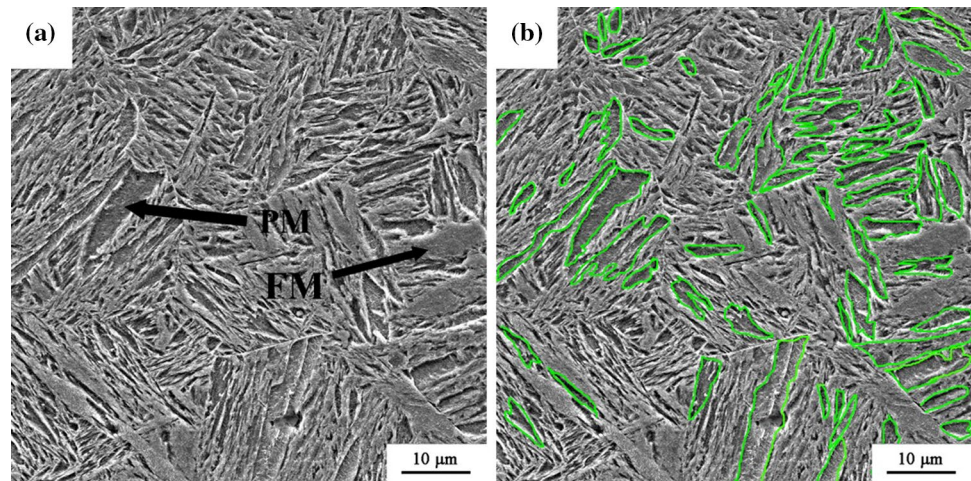

**Table 2** RA content of samples after different cooling processes (%)

	Base steel	Ni-steel	Ni + Cr steel
Isothermal cooling	0	3%	1%
Continuous cooling	0	0	0

The dilation curves of the ITP-treated samples are displayed in Fig. 6a. It is observable that the transformation rate of the base steel was significantly higher (completed in about 200 s) than those of Ni-steel and Ni + Cr steel. The straight increase in dilation before point A signifies martensitic transformation according to authors' previous study [25]. This is proved by microstructure in Fig. 2a, where large amount of tempered martensite appears during isothermal holding. Therefore, the dilation after point A represents bainitic transformation. Further, Ni-steel and Ni + Cr steel experienced no martensitic transformation before isothermal holding process, thus they yielded higher amounts of bainite as compared to the base steel. It is noticeable from Table 1 that the theoretical Bs of Ni + Cr steel was lower than that of Ni-steel; therefore, the chemical driving force required for

the bainitic transformation of Ni + Cr steel was smaller than that of Ni-steel, thus resulting in a relatively slower bainitic transformation rate in Ni + Cr steel (Fig. 2a). Moreover, carbon contents in untransformed austenite started to decrease due to the continuous precipitation of Cr carbides during isothermal holding process, thus causing a decrease in the chemical stability of untransformed austenite in Ni + Cr steel. Hence, the final amount of bainitic transformation in Ni + Cr steel was found to be higher than that of Ni-steel.

The CCP-treated specimens experienced transformation dilatation and cooling shrinkage (Fig. 6b), and bainitic and martensitic transformations occurred during air-cooling after 380 °C. Small amount of austenite first transformed into bainite, and the remaining austenite were converted into martensite during air-cooling; thus the microstructures of the CCP-treated steels mainly consisted of lath martensite (Fig. 2d–f). The dilation decrease caused by cooling shrinkage was the same for all three steel specimens because of the same cooling route. Therefore, the total amount of bainitic and martensitic transformations in the base steel was higher than those Ni-steel and Ni + Cr steel. The rate of transformation and the amount of transformation of base steel is larger

Fig. 5 XRD pattern for Ni-steel at ITP treatment
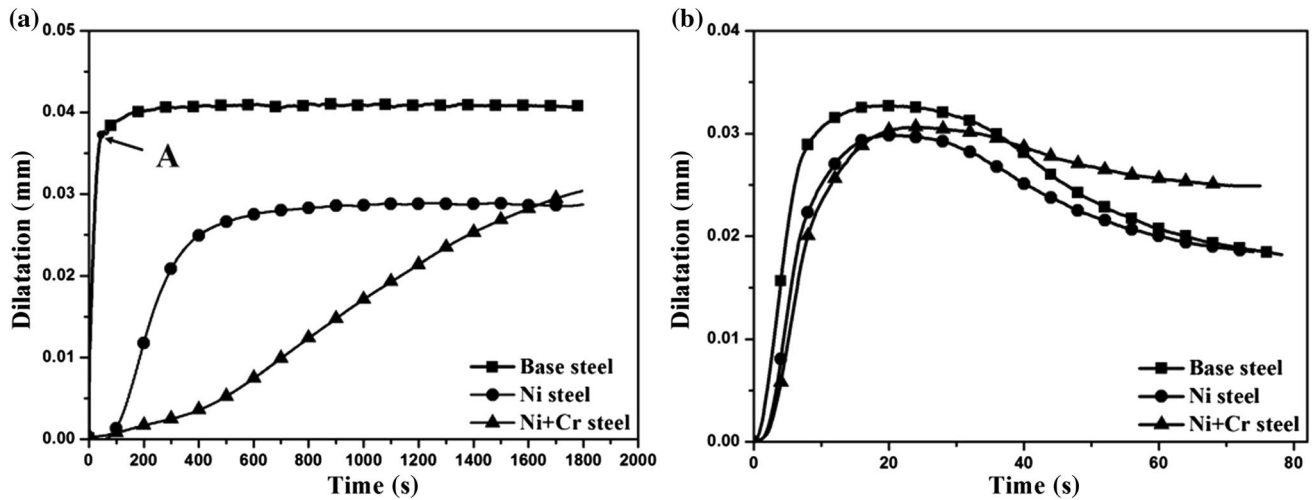
(a)

(b)
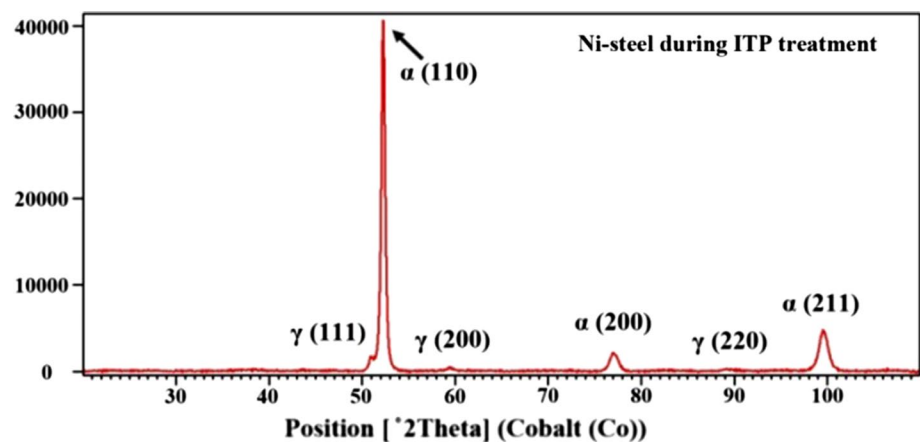
Fig. 6 Diameter change in the samples during different cooling processes after 380 °C: **a** ITP treatment; **b** CCP treatment

than the others. Moreover, although the transformation rate of Ni + Cr steel was lower than Ni-steel, the amount of transformation was larger than Ni-steel.

3.4 Cryogenic Impact Toughness

In order to understand the influence of different cooling processes on CIT of the experimental steels, the V-notch Charpy impact toughness tests were conducted at − 40 °C and the corresponding results are presented in Fig. 7. As compared to the ITP-treated specimens, the CCP-treated specimens manifested better low-temperature impact toughness. The low temperature impact energy of three steels by CCP treatment reached 89 J/cm^2, 99 J/cm^2, and 78 J/cm^2, respectively, suggesting that the steels have larger CIT by CCP treatment. In addition, the CIT is improved by the addition of Ni, while it decreases with composite addition of Ni and Cr.

3.5 Fracture Surface Analysis

The fracture surfaces of the experimental steels were analyzed by SEM (Fig. 8). Both the ITP-treated base steel and Ni-steel manifested a typical brittle fracture with large blocky cleavages (Fig. 8a, b), and some quasi-cleavages were also observed in Ni-steel. Moreover, cracks were formed along the original austenite grain boundaries. In addition, in the fracture morphology of the ITP-treated Ni + Cr steel, dimples were coexistent with quasi-cleavages (Fig. 8c); hence, it yielded higher toughness as compared to the base steel and Ni-steel. Moreover, the volume fraction of BF in base steel during ITP treatment (7.72%) was obviously lower than Ni-steel (44.25%) and Ni + Cr steel (47.66%). Therefore, less amount of BF in base steel led to the brittle fracture. The micro-morphology of the
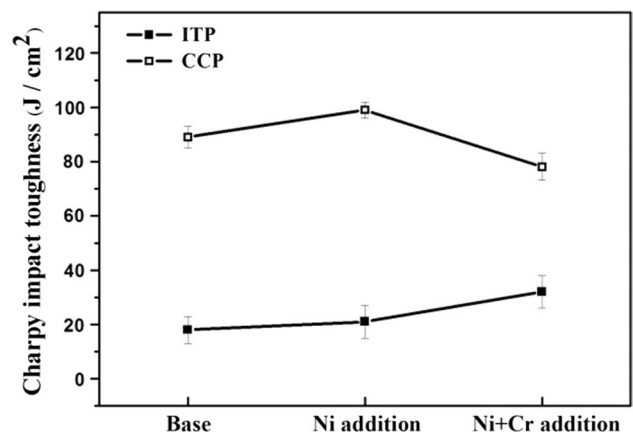

Fig. 7 Charpy impact values of tested steels at − 40 °C (J/cm^2)

fractures is consistent with the volume fractions of BF in three steels by ITP treatment.

However, the CCP-treated steels manifested ductile fracture morphologies (Fig. 8d–f), and fracture surfaces were composed of a large number of ductile dimples. Moreover, in Ni-steel, larger dimples were surrounded by smaller dimples (Fig. 8e), thus indicating that Ni-steel had better low-temperature toughness. However, some strip-dimples and river-like quasi-cleavages were observed in the fractography of Ni + Cr steel (Fig. 8f), meaning that the addition of Cr caused a decrease in low-temperature toughness of Ni + Cr steel. Furthermore, higher volume fraction of PM resulted in the larger impact toughness. The volume fraction of PM in Ni-steel by CCP treatment (23.66%) was higher than that of other steels. Therefore, the micro-morphology of the fracture matches with the
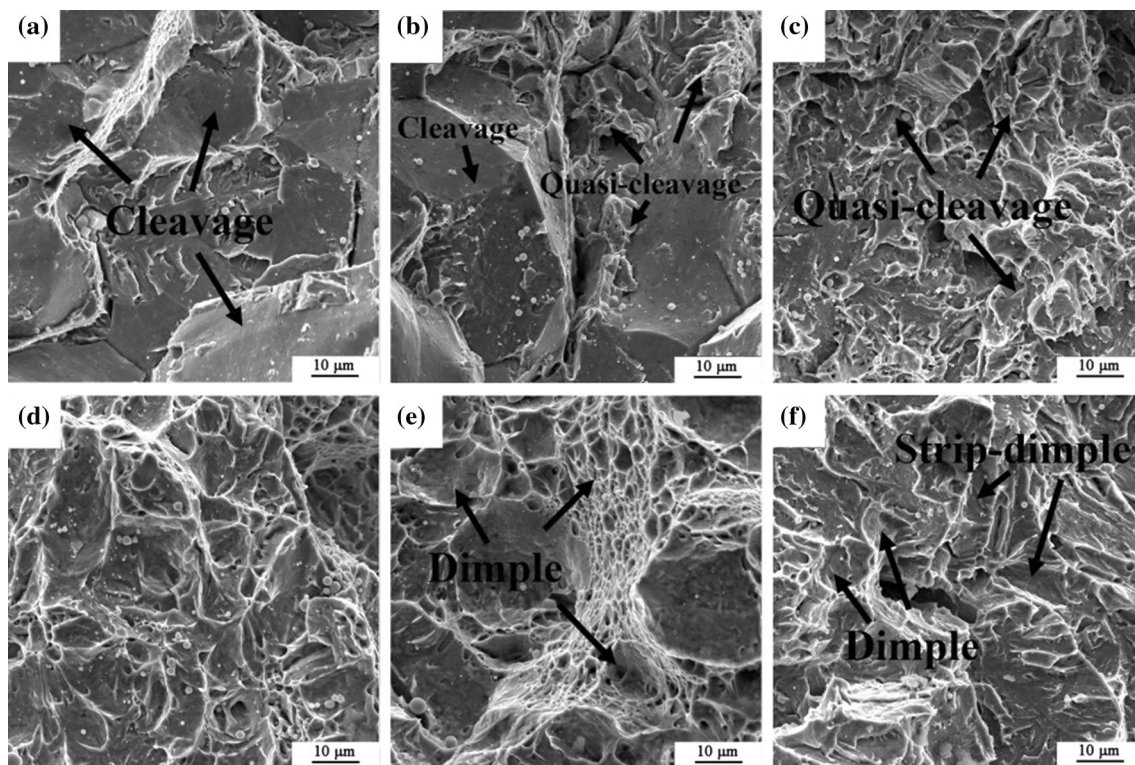
Fig. 8 Fracture surfaces for ITP treatment: **a** base steel; **b** Ni-steel; **c** Ni + Cr steel; and for CCP treatment: **d** base steel; **e** Ni-steel; **f** Ni + Cr steel

results of the impact toughness tests in Fig. 7 and the volume fraction of PM in three steels during CCP treatment.

3.6 Hardness

In the present study, five macro hardness values were averaged to obtain the correct result (Fig. 9). It is evident that Ni had no significant effect on hardness; however, the addition of both Ni and Cr caused a significant increase in macro hardness, which can be attributed to the solid solution of Cr and Ni as well as the fine grain strengthening. Furthermore, Cr is a carbide forming element, thus the precipitation of Cr carbide yields the second phase strengthening effect [29, 30]; hence, the addition of Cr manifested a profound enhancement in macro hardness. Moreover, as the CCP-treated samples contained more LM, their hardness values were found to be much higher than those of the ITP-treated samples.

3.7 TEM Analysis

The CCP-treated specimens manifested higher CIT as compared to the ITP-treated steels (Fig. 7). The results of TEM analysis are presented in Figs. 10, 11, 12 and 13. Figure 10 displays the TEM bright field images of the ITP-treated specimens, and it is discernible that the presence
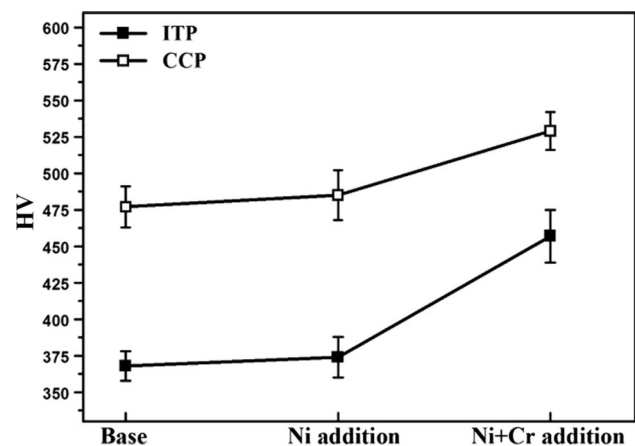

Fig. 9 Hardness of different specimens (HV)

of carbide precipitations in the samples resulted in poor CIT. Figure 10a revealed that a large number of thin-film tempered carbides was distributed along austenite grain boundaries and in grains in the ITP-treated base steel. Carbides led to dislocations and stress concentration, thus crack sources were easily formed at certain stress. Hence, the ITP-treated base steel yielded a significantly lower CIT value and manifested brittle fracture morphology (Fig. 8a).
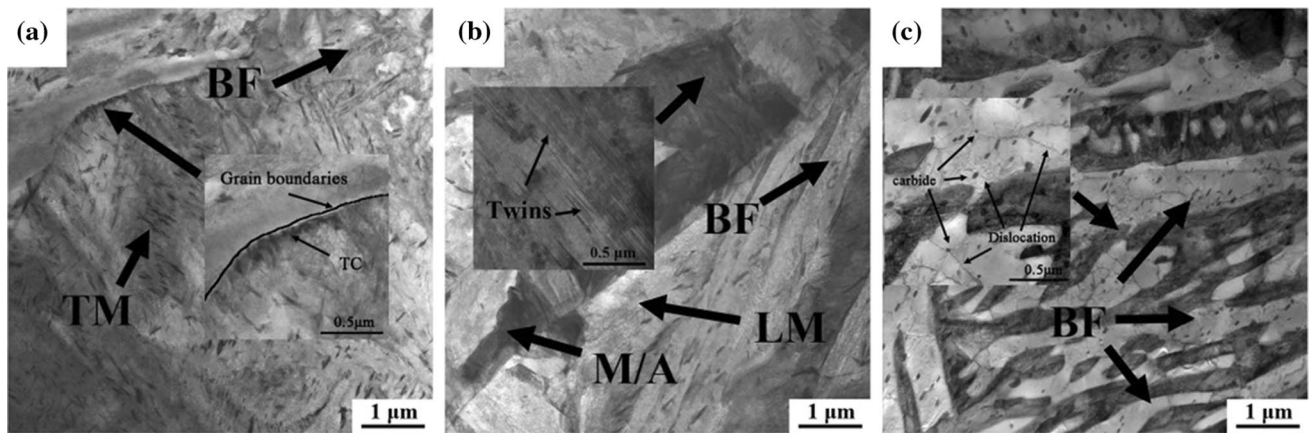
Fig. 10 Bright field TEM images showing the microstructure of specimens for ITP treatment: **a** base steel; **b** Ni-steel; **c** Ni + Cr steel
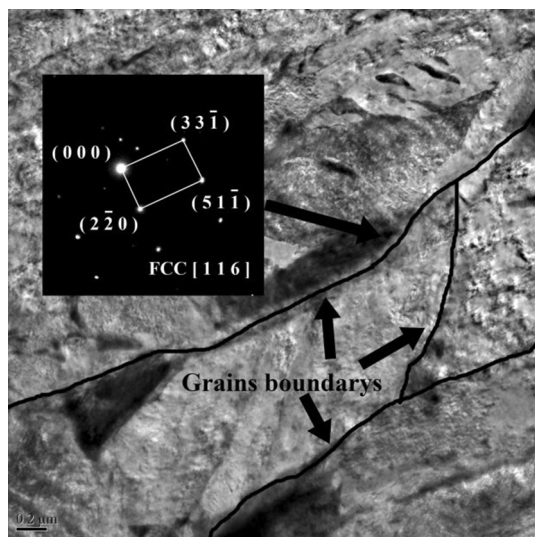

Fig. 11 TEM bright field image of the M/A on the original austenite grain boundary and the corresponding electron diffraction pattern from [1 1 6] zone of one of the γ-Fe retained austenite

XRD results in Table 2 indicate that Ni-steel was composed of 3% RA. Figure 11 displays the homologous selected area electron diffraction (SAED) pattern obtained from one of the dark regions near the grain boundary with [1 1 6] zone and the dark region can be indexed as the face-centered cubic austenite structure (γ-Fe), proving that the dark area in Fig. 11 is RA. Further, twin martensite was formed in the island-like M/A structure (Fig. 10b). As twin martensite possess higher carbon contents, they are difficult to plastically deformation [31–33]. Moreover, the presence of twin martensite along grain boundaries hinders the development of dislocations, and crack sources were easily formed at certain stress. Therefore, the ITP-treated Ni-steel yielded a significantly lower CIT value, and its fracture morphology was dominated by cleavages (Fig. 8b).

The TEM bright field microstructure of the ITP-treated Ni + Cr steel indicates that spheroidized carbide particles were distributed on bainite plates (Fig. 10c). The compositions of carbide particles were detected by EDS point scanning (Fig. 12 and Table 3). The first three spectrums represent carbides, whereas the fourth one signifies the matrix. It is evident that the amounts of Cr and Manganese (Mn) in carbides were significantly higher than those in the matrix, thus indicating the formation of carbide precipitation in Ni + Cr steel during bainitic transformation. However, Ni + Cr steel manifested higher CIT as compared to other two steels, which can be attributed to the fewer carbides and twin martensite along grain boundaries as well as to the existence of fine bainite in its microstructure (Fig. 10c). In addition, according to the calculated volume fractions of BF (7.72%, 44.25% and 47.66% for three steels, Fig. 3) during ITP treatment, the amount of BF in Ni + Cr steel was highest, resulting in a larger CIT value of the ITP-treated Ni + Cr steel.

Figure 9 illustrates the hardness values of the ITP-treated samples. The hardness of the base steel was found to be smaller than other two steel samples. It happened because martensite was tempered at 380 °C during isothermal holding, thus resulting in the decrease in both dislocation density and carbon content. Further, Ni + Cr steel yielded the largest hardness value, which can be attributed to solution strengthening, carbide precipitation strengthening and grain (bainite) refinement strengthening.

Figure 7 reveals that the CCP-treated steels yielded higher CIT values as compared to the ITP-treated samples. Both SEM (Fig. 2) and TEM (Fig. 13) images indicate that the microstructures of the CCP-treated steels mainly consisted of carbide-free bainite and martensite, thus resulting in better CIT values. Moreover, Ni-steel had higher CIT as compared to the base steel; therefore, it can be inferred that Ni-steel contained more bainite because of its lower Ms temperature. The bainitic
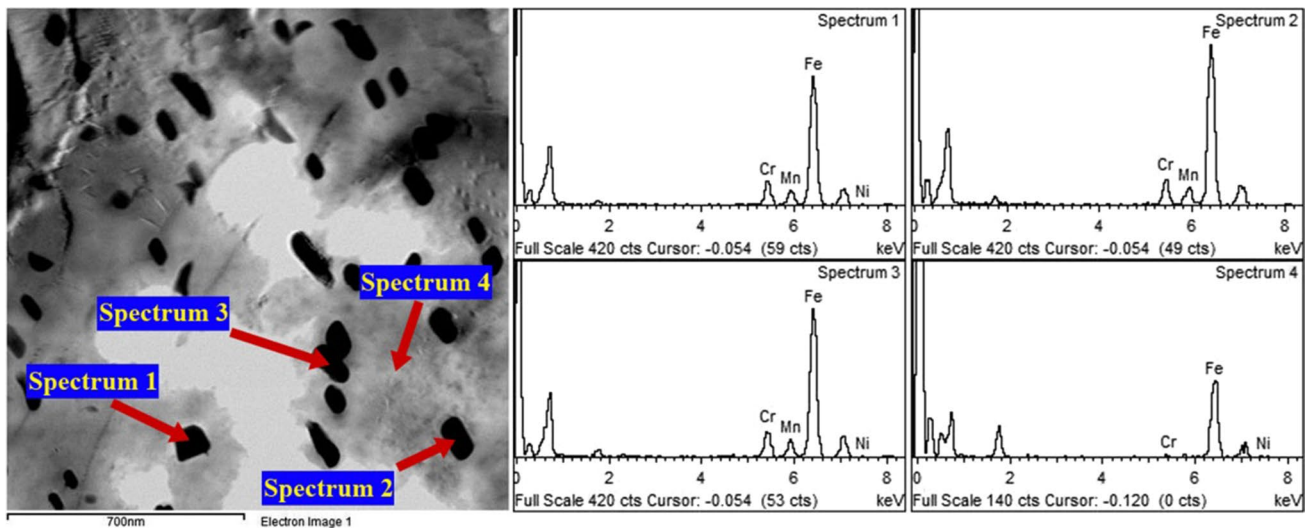
Fig. 12 EDS of carbide particles in Ni + Cr steel by ITP treatment
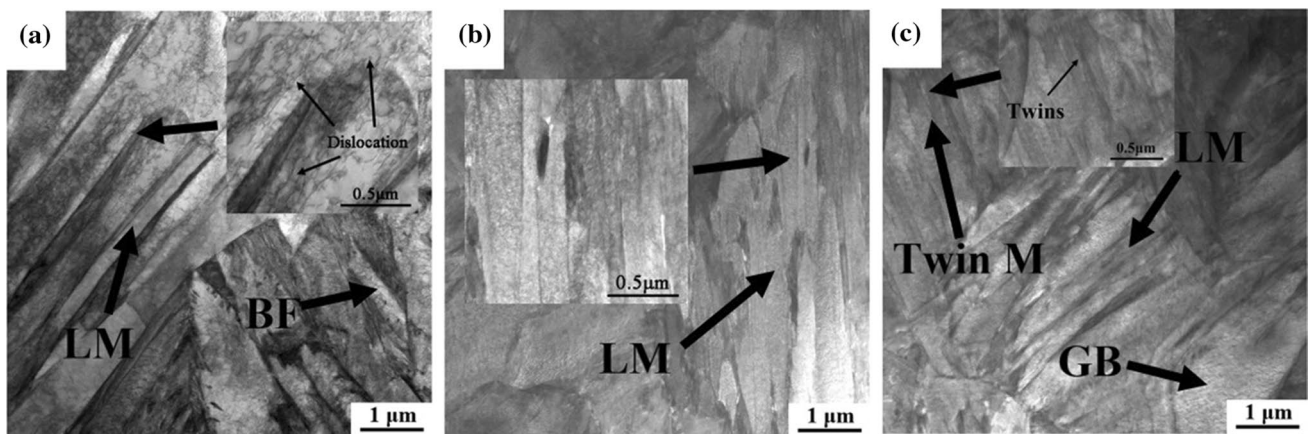

Fig. 13 TEM bright field TEM images showing the microstructure of specimens by CCP treatment: **a** base steel; **b** Ni-steel; **c** Ni + Cr steel

Table 3 Spectral element composition of EDS point scanning (wt%)

Spectrum	Cr	Mn	Fe	Ni	Total
Spectrum 1	13.61	6.48	79.29	0.62	100.00
Spectrum 2	11.45	5.90	82.07	0.58	100.00
Spectrum 3	12.22	5.83	81.32	0.63	100.00
Spectrum 4	2.22	0.13	95.69	1.95	100.00

transformation time of Ni-steel was longer than that of the base steel; hence the addition of Ni manifested a considerable enhancement in CIT, whereas the addition of Ni and Cr caused a decrease in CIT. Figure 13c indicates that the microstructure of Ni + Cr steel consisted of twin martensite and GB. It is well known that GB and twin martensite causes a reduction in toughness [10, 32–34]. Moreover, from the calculated results

(Fig. 4), it is observed that the amount of PM (19.32%) in Ni + Cr steel was smaller than other two steels, leading to a lower CIT value in the CCP-treated Ni + Cr steel.

As the CCP-treated samples had more dislocations in LM, their hardness values were found to be higher than those of the ITP-treated steels (Figs. 10 and 13). The Ni + Cr steel manifested the largest hardness value, which can be attributed to both solution strengthening and the presence of twin martensite in its microstructure.

4 Conclusion

In the present study, three low-carbon high-strength steels of different chemical compositions were designed and treated by two different cooling routes: ITP and CCP. The effects

of Ni and Cr on CIT of the as-prepared steels were investigated by thermal simulation, SEM, TEM, XRD and Charpy impact toughness tests. The following main conclusions can be drawn:

1. As carbide precipitations were suppressed during CCP treatment, the CCP-treated specimens resulted in higher CIT as compared to the ITP-treated specimens.

2. During CCP treatment, the addition of Ni manifested a considerable enhancement in CIT; however, the addition of both Ni and Cr caused a decrease in CIT and an increase in hardness.

3. During ITP treatment, Ni had no significant effects on CIT, whereas the addition of both Ni and Cr caused discernible improvements in both CIT and hardness. However, due to the formation of carbides during isothermal holding, the overall CIT of the ITP-treated steels was poor.

References

1. S.V. Konovalov, V.E. Kormyshev, Y.F. Ivanov, V.E. Gromov, I.A. Komissarova, Mater. Sci. Forum **906**, 101 (2017)
2. Y. Cao, Z.D. Wang, J. Kang, G.D. Wang, J. Iron. Steel Res. Int. **4**, 70 (2013)
3. V.I. Novikov, V.V. Dmitriev, K.I. Nedashkovskii, Met. Sci. Heat Treat. **56**, 159 (2014)
4. M.I. Hartshorne, C. Mccormick, M. Schmidt, P. Novotny, D. Isheim, D.N. Seidman, M.L. Taheri, Metal. Mater. Trans. A **47**, 1517 (2016)
5. D. Delagnes, F. Pettinaristurmel, M.H. Mathon, R. Danoix, F. Danoix, C. Bellot, P. Lamesle, A. Grellier, Acta Mater. **60**, 5877 (2012)
6. H.J. Hu, G. Xu, L. Wang, Z.L. Xue, Y.L. Zhang, G.H. Liu, Mater. Des. **84**, 95 (2015)
7. W. Solano-Alvarez, E.J. Pickering, H.K.D.H. Bhadeshia, Mater. Sci. Eng. A **617**, 156 (2014)
8. H. Lan, L. Du, N. Zhou, X.H. Liu, Acta Metall. Sin. **27**, 19 (2014)
9. W. Yan, L. Zhu, W. Sha, Y.Y. Shan, K. Yang, Mater. Sci. Eng. A **517**, 369 (2009)
10. F.G. Caballero, H. Roelofs, S. Hasler, C. Capdevila, J. Chao, J. Cornide, C. Garcia-Mateo, Mater. Sci. Technol. **28**, 95 (2012)
11. B. Avishan, S. Yazdani, S.H. Nedjad, Mater. Sci. Eng. A **548**, 106 (2012)
12. Z.J. Luo, J.C. Shen, S.U. Hang, Y.H. Ding, C.F. Yang, X. Zhu, J. Iron. Steel Res. Int. **17**, 40 (2010)
13. J. Chakraborty, P.P. Chattopadhyay, D. Bhattacharjee, I. Manna, Metal. Mater. Trans. A **41**, 2871 (2010)
14. D.Y. Liu, H. Xu, K. Yang, B.Z. Bai, H.S. Fang, Acta Metall. Sin. **40**, 882 (2004)
15. M. Wang, Z.Y. Liu, C.G. Li, Acta Metall. Sin. **30**, 48 (2017)
16. P. Wang, K.S. Kumar, Mater. Sci. Eng. A **519**, 184 (2009)
17. L.U. Ma, G.J. Liang, J. Tan, L.J. Rong, Y.Y. Li, J. Mater. Sci. Technol. **15**, 67 (1999)
18. J.Y. Tian, G. Xu, M.X. Zhou, H.J. Hu, X.L. Wan, Metals **7**, 40 (2017)
19. D.D. Shen, S.H. Song, Z.X. Yuan, L.Q. Weng, Mater. Sci. Eng. Ser. A **394**, 53 (2005)
20. S.H. Song, H. Zhuang, J. Wu, Z.X. Yuan, T.H. Xi, Mater. Sci. Eng. A **486**, 433 (2008)
21. C.M. Lin, C.M. Chang, J.H. Chen, W. Wu, Mater. Sci. Eng. A **527**, 5038 (2010)
22. H. Pous-Romero, H.K.D.H. Bhadeshia, Metal. Mater. Trans. A **45**, 4897 (2014)
23. M.N. Yoozbashi, S. Yazdani, T.S. Wang, Mater. Des. **32**, 3248 (2011)
24. M.X. Zhou, G. Xu, H.J. Hu, Q. Yuan, J.Y. Tian, Steel Res. Int. (2016). https://doi.org/10.1002/srin.201600377
25. J.Y. Tian, G. Xu, M.X. Zhou, H.J. Hu, Steel Res. Int. (2010). https://doi.org/10.1002/srin.201700469
26. A.S. Podder, H.K.D.H. Bhadeshia, Mater. Sci. Eng. A **527**, 2121 (2010)
27. J.H. Ryu, D.I. Kim, H.S. Kim, H.K.D.H. Bhadeshia, D.W. Suh, Scr. Mater. **63**, 297 (2010)
28. K. Iwanaga, T. Tsuchiyama, S. Takaki, Key Eng. Mater. **171**, 477 (2000)
29. Z. Oksiuta, N. Baluc, J. Nucl. Mater. **374**, 178 (2008)
30. Y.Y. Song, D.H. Ping, F.X. Yin, X.Y. Li, Y.Y. Li, Mater. Sci. Eng. A **527**, 614 (2010)
31. A. Kostka, K.G. Tak, R.J. Hellmig, Y. Estrin, G. Eggeler, Acta Mater. **55**, 539 (2007)
32. L. Daróczi, S. Gyöngyösi, L.Z. Tóth, D.L. Beke, Scr. Mater. **114**, 161 (2016)
33. P. Boullay, D. Schryvers, J.M. Ball, Acta Mater. **51**, 1421 (2003)
34. P. Zhang, Y. Chen, W. Xiao, D.H. Ping, X.Q. Zhao, Prog. Nat. Sci-Mater. Int. **26**, 169 (2016)